

# Muscle Anatomy-aware Geometric Deep Learning for sEMG-based Gesture Decoding

Adyasha Dash\*, Giulia Zappoli\*, Laya Das, Robert Riener, *Senior Member, IEEE*

**Abstract**—Robust and accurate decoding of gesture from non-invasive surface electromyography (sEMG) is important for various applications including spatial computing, healthcare, and entertainment, and has been actively pursued by researchers and industry. Majority of sEMG-based gesture decoding algorithms employ deep neural networks that are designed for Euclidean data, and may not be suitable for analyzing multi-dimensional, non-stationary time-series with long-range dependencies such as sEMG. State-of-the-art sEMG-based decoding methods also demonstrate high variability across subjects and sessions, requiring re-calibration and adaptive fine-tuning to boost performance. To address these shortcomings, this work proposes a geometric deep learning model that learns on symmetric positive definite (SPD) manifolds and leverages unsupervised domain adaptation to desensitize the model to subjects and sessions. The model captures the features in time and across sensors with multiple kernels, projects the features onto SPD manifold, learns on manifolds and projects back to Euclidean space for classification. It uses a domain-specific batch normalization layer to address variability between sessions, alleviating the need for re-calibration or fine-tuning. Experiments with publicly available benchmark gesture decoding datasets (Ninapro DB6, Flexwear-HD) demonstrate the superior generalizability of the model compared to Euclidean and other SPD-based models in the inter-session scenario, with up to 8.83 and 4.63 points improvement in accuracy, respectively. Detailed analyses reveal that the model extracts muscle-specific information for different tasks and ablation studies highlight the importance of modules introduced in the work. The proposed method pushes the state-of-the-art in sEMG-based gesture recognition and opens new research avenues for manifold-based learning for muscle signals.

**Index Terms**—Domain adaptation, gesture decoding, Riemannian manifold, generalizability.

## I. INTRODUCTION

THE human hand is one of the most versatile and dexterous parts of the human body: it performs numerous activities and gestures achieved through a variety of motion strategies. With rapid development in the fields of wearable sensing, computing, and mechatronics, a plethora of new applications has emerged to restore, enhance and augment the power of the human hand. As an example, intelligent prosthetics allow the control of artificial limbs by decoding movement attempts from muscle physiology [1]. Human-computer interaction (HCI) applications span from entertainment (e.g., virtual reality (VR)-based immersive gaming [2]),

to the healthcare sector (e.g., touchless HCI [3] and VR-based rehabilitation [4]) to the spatial computing field (e.g., real-time gesture-based interaction [5]).

These applications decode the hand movement first, and then drive a visual, auditory, or proprioceptive feedback through peripheral interaction [4]. Movement (or hand gesture) decoding is achieved by processing signals acquired through wearable/nearable sensors such as surface electromyogram (sEMG), camera, etc. Among the available sensing modalities, sEMG-based sensing particularly has been gaining popularity because of its non-invasive nature, the low latency in recording the biosignals and the possibility to record peripheral volitional control signals; these features allow for easy integration with the virtual environment, seamless interaction with the user and a better sense of immersiveness. In addition, availability of low-cost, off-the-shelf sEMG armbands that are safe and easy to use makes sEMG a more lucrative mode of sensing. Thus, considerable research efforts have been dedicated to develop sEMG-based hand gesture decoding algorithms.

### A. Literature review

Hand gesture decoding generally involves two steps - feature extraction and classification. Feature extraction can be achieved through time-domain [6], frequency-domain [7], [8], or time-frequency-domain [8] analysis of the signal. Classification can be achieved with linear discriminant analysis [7], support vector machines [8], etc. However, the sEMG signal, which captures motor unit action potentials (MUAPs), is a non-stationary time series corrupted with sensor noise and movement artifacts, leading to low signal-to-noise ratios (SNR) and containing motion artifacts [9]. Thus, the time-domain and frequency-domain techniques for feature extraction are ill-suited for this problem. Time-frequency analysis (wavelet)-based methods have limitations in capturing long-range dependencies such as slow drifts, fatigue trends, etc. [10] and are sensitive to modeling choices such as order and type of wavelet used [10]. Moreover, the suitability of the above hand-crafted features is greatly dependent on their ability to capture discriminative features from complex action-specific muscle activations and their design requires considerable heuristic knowledge.

Neural network-based methods offer an end-to-end approach for automated feature extraction and classification without the need of human engineering. Convolutional neural networks (CNNs) have been used for sEMG-based gesture classification to capture temporospatiofrequency features through hierarchical feature representation [11]. The superior

A. Dash, G. Zappoli and R. Riener are with the Sensory Motor Systems Lab, Department of Health Sciences and Technology, ETH Zurich, R. Riener is also with SCI Center, Medical Faculty, University of Zurich, Corresponding author's e-mail: addash@ethz.ch).

L. Das was with the Department of Mechanical and Process Engineering, ETH Zurich

\*These authors have equally contributed to the manuscript and share the first authorship.

classification accuracy of CNN-based architectures over classical methods has been well-established in the literature [11], [12]. [12] proposed a novel attention-driven CNN architecture for classifying fine-finger gestures by fusing sEMG with force myogram signal. CNNs have also been combined with long short-term memory (LSTM) [13], [14] with multi-branch processing and bidirectional models to handle long-term dependencies in data. Although these works have achieved state-of-the-art performance, their efficiency has been reported to decrease drastically in case of cross-session scenarios [13] or has not been investigated in such settings [12].

### B. Research gaps

Despite recent progress in neural network-based end-to-end learning for gesture recognition, crucial research gaps still remain largely unaddressed.

1) *Non-Euclidean structure of sEMG*: CNNs are primarily designed for computer vision tasks that assume the input data to be stationary, translation invariant, translation equivariant and stable with respect to local deformations[15], properties that can be verified for data with a Euclidean structure. The same applies for LSTM architectures. However, the sEMG signal, generated as a weighted summation of MUAPs, may not conform to this geometry [16] because of the underlying data generating process. Thus, neural networks built for the Euclidean space can fall short of adequately capturing the relevant information in sEMG. While graph neural network-based approaches [17], [18] address this challenge, the design of the graph, specifically the edge weights, is not straightforward, and the evaluation of these methods is performed on limited number of gestures [18]. Moreover, such non-Euclidean graph neural networks for gesture classification are relatively new and not fully explored in the literature.

2) *Inter-subject and inter-session variability*: An important challenge associated with processing sEMG is the high variability in the signal across subjects and sessions arising from extreme sensitivity to the positioning of electrodes, thickness of subcutaneous fat, spatial distribution of muscle fibers, distribution of muscle fiber conduction velocity, sweating, anatomical/physiological differences between subjects/sessions [19], [11]. The literature has shown that without proper domain adaptive approaches [11] dedicated to handle the distribution shift in sEMG, the decoding performance can decrease by up to 40% [20]. Although recalibration can address this issue, it remains a repetitive and resource-intensive solution. Alternative approaches used to address this domain shift include adaptive learning [11], semi-supervised learning [21] and domain adaptation [20], [22]. These methods suffer from dependence on labeled data or pseudo-labeling schemes on the target domain to perform fine-tuning, which can be viewed as recalibration with a smaller dataset. In addition, these approaches employ Euclidean neural networks and do not consider the non-Euclidean structure of the data.

Thus, a gesture decoding framework that explicitly addresses the non-Euclidean structure of the data and offers generalizability across sessions/subjects without depending on (pseudo)labels is not available in the literature. To address

this gap, we note that covariance-based features, such as common spatial patterns (CSP), based on eigen decomposition of covariance matrices have proven to be superior for gesture classification [23]. Recently, researchers have used geodesic distance between rectified covariance matrices on Riemannian manifold to robustly model complex interactions across spatially distributed motor units during different hand gestures [16]. While manifold-based learning is better-suited to capture the non-Euclidean structure of the data, the methods available in literature rely on hand-crafted features: their design can be inefficient for non-homogeneous sEMG sensor recordings and they are inadequate for modeling the domain shift across subjects/sessions. In this article, we draw inspiration from the success of learning on Riemannian manifolds and develop an end-to-end deep learning model coupled with unsupervised domain adaptation for gesture decoding.

### C. Contributions

In this article, we propose a novel geometric deep neural network, called Temporal-Muscle-Kernel-Symmetric-Positive-Definite Network (TMKNet) on SPD manifold for sEMG-based gesture classification. The contributions of this article are:

- 1) An end-to-end deep neural network model that performs gesture classification in three steps: (1) feature extraction across time and sensors with multiple temporal and spatial kernels, (2) projection of features to the manifold of symmetric positive definite (SPD) matrices, learning on the SPD manifold and projecting back to the Euclidean space, and (3) classification of the hand movement.
- 2) A multi-kernel spatial convolution layer that is informed from the underlying anatomy of gesture execution to extract relevant information for different types of movements.
- 3) An unsupervised domain adaptation layer that uses domain-specific batch normalization for gesture classification from sEMG data.
- 4) Demonstration of superior performance of TMKNet with two datasets (NinaproDB6 and Flexwear-HD) and generalizability of the model in the multi-session scenario.

The remainder of the paper is organized as follows: Section II introduces the preliminary concepts used to develop TMKNet. Section III provides a detailed description of the proposed method. The experimental setup is detailed in Section IV and the results are provided in Section V. Section VI provides a discussion and concluding remarks.

## II. PRELIMINARIES

In this section, we introduce the concepts and notation used in article.

### A. Riemannian geometry

sEMG data exhibits non-Euclidean structure, and the notions of quantities like distance, mean and variance that are defined in the Euclidean space must be revised according to the structure of the data. We make use of the SPD manifold,

which belongs to a class of popularly studied manifolds called Riemannian manifolds. We describe these quantities for such manifolds.

A Riemannian manifold ( $\mathcal{M}$ ) is a smooth manifold equipped with an inner product on the tangent space  $\mathcal{T}_Z\mathcal{M}$  at each point  $Z \in \mathcal{M}$ .  $\mathcal{T}_Z\mathcal{M}$  has a Euclidean structure with easy-to-compute distances that locally approximate Riemannian distances (on  $\mathcal{M}$ ), i.e., Affine Invariant Riemannian Metric (AIRM), on  $\mathcal{M}$  induced by an inner product. Mathematically, the distance between two points  $Z_1$  and  $Z_2$  on  $\mathcal{M}$  computed in AIRM is defined as:

$$\delta_{\text{AIRM}}(Z_1, Z_2) = \left\| \log \left( Z_1^{-\frac{1}{2}} Z_2 Z_1^{-\frac{1}{2}} \right) \right\|_F, \quad (1)$$

where  $\|\cdot\|_F$  is the Frobenius norm. For a set of points  $Z = \{Z_j \in \mathcal{M}\}_{j \leq K}$ , the mean of  $Z$  on the manifold is called Fréchet mean ( $G_Z$ ), and the variance of  $Z$  on the manifold is called Fréchet variance ( $V_Z^2$ ).  $G_Z$  is the point that minimizes the inertia with respect to  $Z$  and can be obtained as:

$$G_Z = \arg \min_{G \in \mathcal{M}} \frac{1}{K} \sum_{j=1}^K \delta_{\text{AIRM}}^2(G, Z_j). \quad (2)$$

For  $K = 2$ ,  $G_z$  has a closed-form solution:

$$G_Z(Z_1, Z_2; w) = Z_1 \#_w Z_2 = Z_1^{\frac{1}{2}} \left( Z_1^{-\frac{1}{2}} Z_2 Z_1^{-\frac{1}{2}} \right)^w Z_1^{\frac{1}{2}}. \quad (3)$$

Here,  $\#_w$  : denotes weighted geometric mean operator for the weight  $w$ . For  $K > 2$ , there exists no closed-form solution, and  $G_Z$  is estimated through an iterative process, referred to as Karcher flow, which projects the data to the tangent space at the current estimate, performs arithmetic averaging and then projects them back to the manifold. The Fréchet variance  $V_Z^2$  is obtained as

$$V_Z^2 = \frac{1}{K} \sum_{j=1}^K \delta_{\text{AIRM}}^2(G, Z_j). \quad (4)$$

These quantities are used in the forward and backward pass calculations in Riemannian neural networks.

### B. Unsupervised domain adaptation

Domain adaptation aims at building a model that is trained with data from one or more source domains, and can generalize to one or more target domains. Let  $\mathbf{S} = \{S_i\}_{i=1}^{N_s}$  represent the set of  $N_s$  source domains and  $\mathbf{T} = \{T_j\}_{j=1}^{N_t}$  represent the set of  $N_t$  target domains. Let us denote the input features and label for the  $i^{\text{th}}$  source domain and  $j^{\text{th}}$  target domain as  $\{X_{S_i}, Y_{S_i}\}$  and  $\{X_{T_j}, Y_{T_j}\}$ , respectively. In this article, we adopt an unsupervised domain adaptation (UDA) approach, which aims to build a model that is trained with  $\{X_{S_i}, Y_{S_i}\}_{i=1}^{N_s}$  and generalizes to all  $X_{T_j}$  without using the label information  $\{Y_{T_j}\}_{j=1}^{N_t}$ . In contrast to (semi-)supervised domain adaptation, UDA does not rely on labels  $\{Y_{T_j}\}_{j=1}^{N_t}$  or pseudo-labels, and thus, is cost-efficient, scalable to new domains and tasks, and has better real-world applicability, where labelled data for each new subject/session is unavailable.

### C. Riemannian Batch Normalization

Batch normalization (BN) is a method that minimizes the covariate shift in the data and features by smoothing the distribution to speed up convergence. In the Euclidean space, BN involves centering and scaling operations realized through subtraction and division. However, on manifolds, these operations are achieved through parallel transport. For a vector  $S$  on the tangent space of  $Z_1$ , the parallel transport operation  $\Gamma_{Z_1 \rightarrow Z_2}(S)$  between  $Z_1, Z_2 \in \mathcal{M} = S^{++}$  (SPD manifold) defines a path from  $Z_1$  to  $Z_2$  through projection on tangent bundles (set of tangent spaces) while  $S$  remains parallel to itself in the tangent spaces along the path as follows:

$$\forall S \in \mathcal{T}_{Z_1}; \Gamma_{Z_1 \rightarrow Z_2}(S) = (Z_2 Z_1^{-1})^{\frac{1}{2}} S (Z_2 Z_1^{-1})^{\frac{1}{2}} \in \mathcal{T}_{Z_2} \quad (5)$$

In the context of Riemannian batch normalization (RBN), the Fréchet mean of the  $l^{\text{th}}$  batch  $B_l$ , denoted as  $G_{B_l}$  can be approximated as proposed in [24] by using Karcher flow with only one iteration. Parallel transport can then be used to normalize with a bias parameter  $G_\phi$  and variance parameter  $V_\phi^2$  as follows [24],[25]:

$$\text{SPDBN}(Z_j; G_\phi, V_\phi^2, \epsilon) = \Gamma_{I \rightarrow G_\phi} \left( \Gamma_{G_{B_l} \rightarrow I}(Z_j)^{\frac{V_\phi}{V_{B_l} + \epsilon}} \right) \quad (6)$$

Batch-specific statistics during training can induce noise whose level depends on batch size, and is more pronounced for smaller batches. To combat this, SPD momentum batch normalization is used, where the algorithm uses two sets of statistics (Fréchet mean) separately for training and testing that are updated with momentum parameters. In SPD momentum batch normalization (SPDMBN) [25],  $\gamma_{\text{source}}, \gamma_{\text{target}} \in [0, 1]$  are clamped exponential decay scheduler parameters for source and target domains.

## III. METHODOLOGY

In this section, we propose a generalizable system-informed geometric deep neural network TMKNet for sEMG-based gesture classification. TMKNet consists of three stages, namely, (1) Multi-scale system-inspired feature extraction stage, (2) SPD Network and domain-specific batch-normalization stage, and (3) Classification stage. The detailed architecture of TMKNet is given in figure.

Let us denote an sEMG signal as  $X \in \mathbb{R}^{c \times t}$  where  $c$  and  $t$  represent the number of channels (sensors) and number of samples, respectively. The proposed model takes as input, a batch of examples  $X_{\text{batch}} = [X_1, X_2, X_3, \dots, X_b] \in \mathbb{R}^{b \times c \times t}$  and passes them through Euclidean and Riemannian layers to classify the movement. In the following, we present a detailed description of each layer in the proposed model.

### A. Euclidean Stem

The first module consists of multiple Euclidean layers that extract features at multiple spatio-temporal resolutions from the input sEMG signal, designed with inspiration from theory of muscle physiology, signal processing and human anatomy.

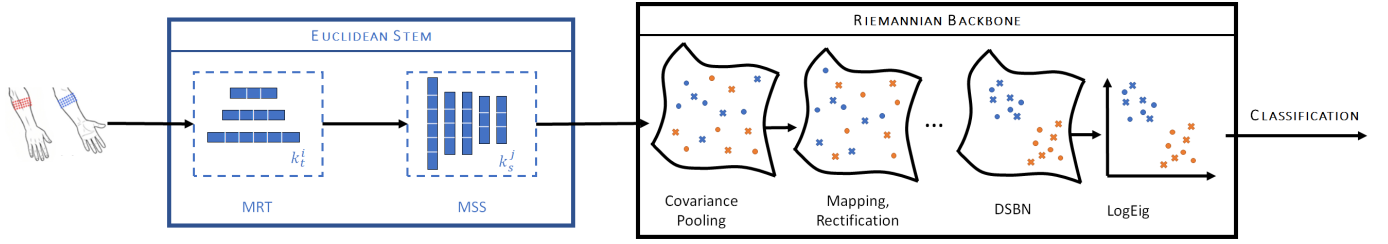


Fig. 1. Proposed end-to-end Riemannian network for gesture classification from sEMG. The multi-channel data is fed to the Euclidean stem for multi-scale temporal and spatial feature extraction with kernels  $k_t^i$  and  $k_s^j$ , respectively. The features are transformed to SPD manifold, processed on manifolds and transformed back for final classification. Markers represent domains (subjects/sessions) and colours represent classes.

1) *Multi-resolution temporal layer (MRT)*: sEMG signal being a non-stationary signal with varying frequency content, the time-frequency information at varying resolutions can provide important discriminative power for classifying the sEMG signal. The MRT layer is a composite layer consisting of multiple 1-D convolution layers with different kernel sizes designed to extract the time-frequency information at varying resolutions from the signal. The size of the temporal kernels are calculated from the sampling frequency ( $F_s$ ) of the signal. The size of the  $i^{th}$  temporal kernel, denoted as  $k_t^i$  is:

$$k_t^i = (1, \alpha_i F_s) \quad (7)$$

where,  $i$ , represents the index of the kernel,  $\alpha_i = r_{data} \cdot r_{resolution,i}$  is the scaling factor for the  $i^{th}$  kernel that includes dataset-specific and dataset-independent ratios,  $r_{data}$  and  $r_{resolution,i}$ , respectively. Longer kernels can capture long-range dependencies and low frequency variations, while shorter kernels can extract high-frequency information from the signal. By including multiple 1-D convolution layers with varying kernel sizes  $k_t^i$ , we aim to capture information at multiple frequency resolutions from the sEMG signal. The output of each kernel is passed through a LeakyReLU activation that introduces nonlinearity and then downsampled using a MaxPooling layer to reduce the effect of noise and mitigate the curse of dimensionality. These are stacked together along the feature dimension and passed through a Euclidean batch normalization layer to minimize the covariate shift problem. The operations performed by the MRT layer can be expressed as:

$$z_t^i = \text{MaxPool}(\text{LeakyReLU}(\text{Conv1D}(X, k_t^i))) \quad (8)$$

$$Z_t = \text{BatchNorm}(\text{Stack}(\{z_t^i\})) \quad (9)$$

The final output of the MRT layer is  $Z_t \in \mathbb{R}^{b \times n_t \times c \times t_t}$ , where  $n_t$  represents the number of output channels of the MRT layer. The last dimension is equal to the sum of the corresponding sizes of individual  $z_t^i$ .

2) *Multi-scale Spatial Layer (MSS)*: At an anatomical level, different hand gestures are executed by the collective functioning of flexor and extensor muscles, and are manifested as different coactivation patterns in the sEMG signal. The multi-scale spatial layer is the second composite layer that extracts patterns from different channels of the output of the MRT layer, and is composed of the following kernels:

1) Global muscle kernel, with size  $k_s^1 = (c, 1)$  that processes all the channels together.

- 2) Flexor muscle kernel, with size  $k_s^2 = (c/2, 1)$  that processes the channels corresponding to flexor muscles.
- 3) Extensor muscle kernel, with size  $k_s^3 = (c/2, 1)$  that processes the channels corresponding to extensor muscles.
- 4) Proximal-Distal muscle kernel, with size  $k_s^4 = (c/2, 1)$  and a stride of  $c/2$  that processes all proximal muscle sensors together, followed by all distal muscle sensors together.
- 5) Dilated kernel, with size  $k_s^5 = (2, 1)$  and dilation factor of  $c/2$ .

The outputs of all the layers are passed through LeakyReLU activation and then stacked together before passing through a batch normalization layer. The operations performed by the MSS layer can be expressed as:

$$z_s^j = \text{LeakyReLU}(\text{Conv1D}(X, k_s^j)) \quad (10)$$

$$Z_s = \text{BatchNorm}(\text{Stack}(z_s^1, z_s^2, \dots, z_s^5)) \quad (11)$$

The final output of the MSS layer is  $Z_s \in \mathbb{R}^{b \times n_s \times c_s \times t_t}$ , where  $n_s$  represents the number of output channels of the MSS layer. The last dimension is equal to the sum of the corresponding sizes of individual  $z_s^j$ .

## B. Riemannian Backbone

The Euclidean stem extracts features from the sEMG signal that lie in the Euclidean space. The Riemannian backbone first projects these Euclidean features onto a Riemannian manifold, specifically the SPD manifold and then extracts features on manifolds while preserving the underlying geometric structure. In the following, we describe the different layers that constitute the Riemannian backbone.

1) *Covariance Pooling Layer*: To transform the Euclidean features extracted by the MSS layer, we calculate the covariance of the features, that lie on the SPD manifold. The covariance matrix captures the second-order information in the extracted features and is a powerful tool to analyze multivariate sEMG data where functional connectivity between different muscles carries vital information. This layer takes the flattened features  $\tilde{Z}_s \in \mathbb{R}^{b \times n_s \times c_s \times t_t}$  as input and computes the covariance matrix along the channel dimension. The covariance matrix is a positive definite matrix if the individual vectors are linearly independent. To ensure that the output of this layer

always lies on the SPD manifold, a regularization is performed as follows:

$$\tilde{C} = \text{cov}(\tilde{Z}_s) \quad (12)$$

$$C = \tilde{C} + \lambda I \quad (13)$$

The final output of the covariance pooling layer,  $C \in \mathcal{S}_{n_s}^{++} \subset \mathbb{R}^{b \times n_s \times n_s}$  lies on the SPD manifold  $\mathcal{S}_{n_s}^{++}$ .

2) *BiMap Layer*: The input covariance matrix can have high dimension due to a large number of features. The BiMap layer performs dimensionality reduction of covariance matrices while ensuring the positive definiteness using a bilinear mapping. This involves multiplying the input covariance matrices with a full-rank matrix  $W$  through a bilinear operation as follows:

$$H_{bimap} = WCW^T \quad (14)$$

The output of the BiMap layer,  $H_{bimap} \in \mathcal{S}_{n_b}^{++}$  lies on the SPD manifold with  $n_b < n_s$ . In order to ensure that  $H_{bimap}$  lies on an SPD manifold, the weight matrix  $W$  is required to lie on a compact Stiefel manifold.

3) *ReEig Layer*: This layer is used to introduce non-linearity to the Riemannian module of the network by eigenvalue rectification. It clamps the eigenvalues of the input SPD matrices smaller than a threshold and then reconstructs the matrix. This is inspired by the rectified linear unit operation, common in Euclidean networks. This operation resembles nonlinear filtering on the input features, which can improve the expressive capacity of the module. The operations performed by the layer can be expressed as:

$$H_{bimap} = U_b S_b U_b^T \quad (15)$$

$$H_{reeig} = U_b \max(\epsilon I_{n_b}, S_b) U_b^T \quad (16)$$

Here,  $\epsilon$  is the rectification threshold and  $I_{n_b}$  is the identity matrix of dimension  $n_b$ .

4) *Domain-specific Batch Normalization Layer*: This layer performs unsupervised domain adaption on SPD manifold. This layer separates domain-specific information from the data in the form of BN statistics (mean and variance) and transforms the domain-specific data to domain-invariant data. It consists of multiple BN layers where each layer is devoted to one domain and captures domain-specific data statistics (mean and variance) to normalize the data accordingly.

For a fixed batch size of  $b$ , batches are generally constructed with the same number of examples from different domains, so that the domains are uniformly represented. Since the batch size is fixed during training, an increase in the number of source domains leads to less number of samples per domain, and higher batch-specific noise. Thus, momentum DSBN is proposed, where two sets of running Fréchet mean is computed for each domain to be used in training and testing phase respectively. We construct this layer with multiple SPD batch normalization layers with momentum that have dedicated momentum parameters  $\gamma_{source}$  and  $\gamma_{target}$  for source and

target domains, respectively. The operations performed by this layer can be expressed as:

$$H_{reeig} = \begin{bmatrix} H_{reeig,S_1}, H_{reeig,S_2}, \dots, H_{reeig,S_{n_s}}, \\ H_{reeig,T_1}, H_{reeig,T_2}, \dots, H_{reeig,T_{n_t}} \end{bmatrix} \quad (17)$$

$$H_{bn,S_i} = \text{SPDMBN}(H_{reeig,S_i}, G_\phi, V_\phi^2, \epsilon, \gamma_{source}) \quad \forall i \in \{1, 2, 3, \dots, n_s\} \quad (18)$$

$$H_{bn,T_j} = \text{SPDMBN}(H_{reeig,T_j}, G_\phi, V_\phi^2, \epsilon, \gamma_{target}) \quad \forall j \in \{1, 2, 3, \dots, n_t\} \quad (19)$$

$$H_{dsbn} = \begin{bmatrix} H_{bn,S_1}, H_{bn,S_2}, \dots, H_{bn,S_{n_s}}, \\ H_{bn,T_1}, H_{bn,T_2}, \dots, H_{bn,T_{n_t}} \end{bmatrix} \quad (20)$$

5) *LogEig Layer*: This layer projects the SPD matrices onto the tangent space of  $\mathcal{S}_{n_b}^{++}$ , which is a Euclidean space. This is achieved by replacing the eigenvalues of the matrix by their logarithms and reconstructing the matrix as follows:

$$H_{reeig} = U_r S_r U_r^T \quad (21)$$

$$H_{logeig} = U_r \log(S_r) U_r^T \quad (22)$$

The final output of the module,  $H_{logeig} \in \mathbb{R}^{b \times n_b \times n_b}$  is then processed by the classification head for gesture recognition.

### C. Classification head

The final module consists of a flattening layer that transforms the matrix into a vector, followed by linear probing for classification, as follows:

$$Z = \text{Flatten}(H_{logeig}) \quad (23)$$

$$l = \text{Linear}(Z) \quad (24)$$

The final output of this module,  $l \in \mathbb{R}^{b \times n_c}$  represents the unnormalized logits for  $n_c$  classes predicted by the model.

## IV. EXPERIMENTAL SET-UP

### A. Datasets and preprocessing

We evaluate the proposed approach on two publicly available gesture recognition datasets: (1) NinaproDB6 [26], and FlexWear-HD [22]. Both the datasets contain data from multiple subjects and sessions with drift in distributions across sessions and subjects. These datasets have previously been cited as valuable resources for analyzing practical measures of out-of-distribution performance for EMG datasets [22].

1) *NinaproDB6*: This dataset has 12 repetitions (each repetition referred as a trial) of 7 object grasping actions executed with 14 real-life objects. The sEMG data was collected with 14 Delsys Trigno sEMG electrodes with sampling frequency of 2000 Hz. The sEMG sensors are placed in two rows in the forearm covering both flexor and extensor muscles. The dataset comprises 10 subject data with each subject recorded twice (2 sessions) per day over a period of 5 days.

We adopt the preprocessing approach presented in [26]. At first, the sEMG data is synchronized. The data is then labeled and augmented with a 200 ms rolling window with 100 ms overlap; a Hampel filter is applied on each window to remove powerline interference at 50 Hz. This process results in 156408 trials of 200 ms each. The resulting trials are z-score normalized.

2) *FlexWear-HD*: This dataset consists of 10 hand gestures from 13 subjects with 2 sessions per subject in a single day. The sEMG data was collected using an array of 64 hydrogel electrodes with gold-plated copper pads from the forearm covering both flexor and extensor muscles at 4000 Hz. 8 – 10 repetitions and 4 – 5 repetitions per gesture were taken in the first and second session, respectively. We adopt the preprocessing steps presented in [22]. Each trial passes through a 250 ms sliding window with 125 ms overlap for trial augmentation. Each resulting trial is then passed through a 50 Hz Hampel filter for power line noise cancellation and Z-score normalized. The total number trials generated after augmentation is 31185.

### B. Evaluation baseline, metrics and scenarios

This article proposes the first geometric deep neural network designed for sEMG-based gesture decoding. So, we compare its performance with a geometric network that was previously developed for motor imagery classification with EEG signals, called TSMNet [25].

We evaluate and compare the performance of TMKNet using classification accuracy and F1 score. The accuracy is computed as the ratio of correctly predicted samples to the total number of samples which is well-suited for class-balanced datasets. In our case, FlexWear-HD is class-imbalanced, so we compute F1 scores which is better-suited for class-imbalanced dataset. In order to compare the statistical relevance of the results, we used non-parametric Wilcoxon signed-rank test for F1 scores and accuracies of the TSMNet and TMKNet.

The efficacy of the TMKNet is evaluated in the intersession setting with a leave-one-out approach, where training is performed on all sessions except one of a specific subject and the left-out session is used for testing.

### C. Implementation details

The code is implemented in PyTorch library and the source code is available at [github.com/gzappoli/UDA-sEMG](https://github.com/gzappoli/UDA-sEMG). The Euclidean stem consists of one MRT and one MSS layer with  $r_{data}$  is set to  $\frac{1}{5}$  for NinaproDB6 and  $\frac{1}{4}$  for FlexWear-HD dataset, and  $r_{resolution,i}$  is set to  $\{\frac{1}{16}, \frac{1}{32}, \frac{1}{64}\}$ , for  $i = \{1, 2, 3\}$ , respectively. For NinaproDB6 and FlexWear-HD respectively, the global muscle kernels length are 14 and 64, the flexor and extensor muscle kernel lengths are 7 and 32, the proximal-distal muscle kernel sizes are 7 and 32, the size of dilated kernel is 2 with dilation factor of 7 and 32. In our experiments,  $n_t = 64$ ,  $n_s = 40$  and  $n_b = 30$  for both datasets. The Riemannian backbone consists of one covariance pooling layer followed by a BiMap layer, a ReEig layer, a domain-specific batch normalization layer and a LogEig layer.

The batch size is 50 for both datasets. The number of domains per batch is 5 and 1 for NinaproDB6 and FlexWear-HD respectively. These hyperparameters are the same for all the subjects and sessions. The RiemannianAdam optimizer from Geopt toolbox [27] is used and the cross entropy loss with learning rate 0.001 and weight decay 0.0001 is used for training.

## V. RESULTS

In this section, we first present the performance of the proposed model for gesture classification and compare it with a TSMNet model [25] trained with sEMG data for both datasets. We then present a visual representation of the features extracted by the Euclidean stem. We also highlight the role of the domain-specific batch normalization layer in performing unsupervised domain adaptation on the Riemannian manifold. Finally, ablation studies demonstrate the importance of different layers in the model.

### A. Performance of TMKNet

Table I presents the classification accuracies and F1 scores of the proposed model averaged across all participants for both datasets. TMKNet outperforms UDA-based methods in the literature that use Euclidean networks that do not use target label information for fine-tuning ( $0.6152 \pm 0.1159$ ,  $0.6169 \pm 0.1191$ ,  $0.6012 + 0.1282$  [28]) for the Ninapro-DB6 dataset by at least 8.83 points in terms of accuracy. As the Flexwear dataset is relatively new, there is no literature to compare with for the intersession-setting.

We also compare the performance of TMKNet with TSMNet for both datasets and report them in Table I. We achieve an improvement of 4.63 points in accuracy and 4.69 points in F1 score for the NinaproDB6 dataset. The corresponding numbers are 0.15 (accuracy) and 0.18 (F1 score) for Flexwear-HD dataset. We further highlight that the standard deviation for accuracy is lower for the proposed model, confirms that our proposed network provides more robust prediction. A similar observation is found for the F1 score metric that confirms that the prior observation on accuracy can be transferred to the F1 score. The subject-wise average accuracies for both the datasets are shown in Fig. 2, which presents a more detailed view of the performance of the two models. It can be observed that for NinaproDB6 datasets, all subjects show an improved accuracy and F1 score with our model, and for FlexWear-HD dataset, the majority of subjects show improved accuracy and F1 scores.

In order to investigate the statistical relevance of the observed results, we performed the non-parametric Wilcoxon signed-rank test considering the non-normal distribution of data. We observed that for NinaproDB6 dataset, both the metrics are found to be statistically significantly better with TMKNet with  $p < 0.0001$ . This observation confirms that the TMKNet performs better than the adapted TSMNet for NinaproDB6 dataset. However, for Flexwear-HD dataset, the observed differences are not significant. This is potentially due to the lower number of sessions (2) for this dataset compared to NinaproDB6 (10). In addition, it is also noteworthy that the TSMNet metric values are considerably high with a perfect 100% score within on standard deviation of the mean metric. Thus, achieving statistically significant results with higher performance than TSMNet is difficult. Nevertheless, we observe a improved accuracy and F1 scores in case of majority number of participants.

TABLE I  
 INTER-SESSION CLASSIFICATION ACCURACY AND F1 SCORE OF TSMNET TMKNET FOR NINAPRODB6 AND FLEXWEAR-HD DATASETS. **BOLD** ENTRIES REPRESENT THE BEST PERFORMANCE OF THE TWO MODELS.

Dataset	TSMNet		TMKNet	
	Accuracy	F1	Accuracy	F1
NinaproDB6	0.6623 ± 0.1405	0.6581 ± 0.1408	<b>0.7086 ± 0.1332</b>	<b>0.7050 ± 0.1335</b>
FlexWear-HD	0.9794 ± 0.0211	0.9787 ± 0.0218	<b>0.9809 ± 0.0168</b>	<b>0.9805 ± 0.0170</b>

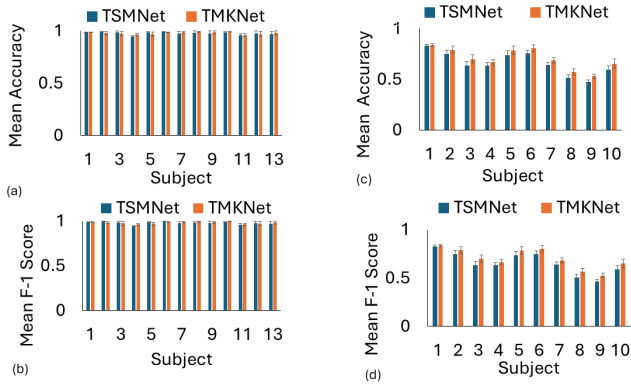


Fig. 2. Subject-wise inter-session classification accuracy and F1 score with TMKNet and TSMNet (a) accuracy for FlexWear-HD dataset, (b) F1 score for Flexwear-HD, (c) Accuracy for NinaproDB6 dataset, (d) F1 score for NinaproDB6 dataset

B. Interpretability

We obtain the saliency maps of the input channels, calculate the sensor-wise maximum saliency over time and plot them in Fig. 3 for two typical and complementary tasks, i.e., wrist extension and wrist flexion for subject 1, session 1 of the Flexwear-HD dataset. It can be observed from Fig. 3 that the saliency for extensor sensors are higher (in blue) for the extension task, while those for the flexion sensors (in orange) are higher for the flexion task.

A detailed analysis reveals that for the extension task, the top 10 important channels are found to be 30, 44, 31, 46, 47, 25, 45, 61, 34, 28, all of which are located near the posterior side of the hand and capture sEMG from extensor muscles. Specifically, sensors 30, 31 are placed (in middle) near extensor carpi radialis longus (ECRL) muscle which is important for functional wrist extension tasks. On the other hand, for flexion task, channels 19, 39, 1, 20, 31, 17, 49, 61, 47, 34 are the top 10 important channels, of which, 7 sensors are placed in the anterior side of the forearm, covering flexor muscles near flexor carpi radialis (FCR) and 3 sensors placed on the posterior side covering the extensor muscles. This is in line with the observation in the literature that for wrist flexion task, the flexor muscles are more active than the extensor muscles, with some extensors muscles activating as a synergist to stabilize the movement [29]. Thus, the model extract features from sensors that are in agreement with the underlying mechanisms of hand movement.

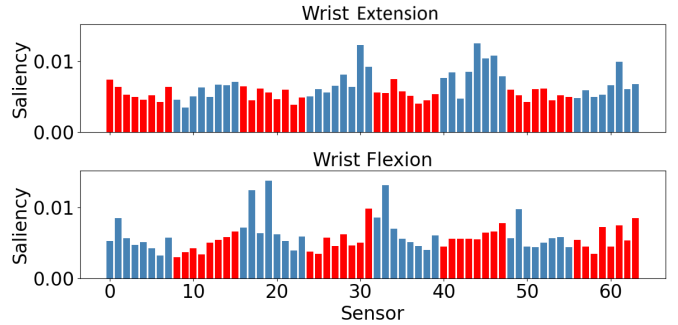


Fig. 3. Sensor-wise maximum saliency for wrist extension and flexion tasks for a sample subject and session in Flexwear-HD dataset.

C. Effect of domain-specific batch normalization

To highlight the importance of the domain-specific batch normalization layer of TMKNet, we use t-distributed Stochastic Neighborhood Embedding (t-SNE) [30] to generate 2D projections of the outputs of the intermediate layers in TMKNet. Fig. 4 compares the t-SNE of the features before and after the domain-specific batch normalization layer in TMKNet for the Nianapro-DB6 dataset. The plot comprises data from both source and target domains for a sample subject (subject 1), with session 9 as the target domain. It can be observed from Fig. 4 that prior to batch normalization, the samples within a class (e.g., blue data points in Fig. 4) exhibit many patches, exhibiting poor localization. For some classes, samples from different domains, i.e., markers are segregated from others (e.g., cross marker for orange data points), showing poor domain-invariance of the features. The samples also overlap across classes (e.g., orange and red data points in Fig. 4). After the batch normalization layer, which performs normalization specific to each domain, the data belonging to each class are better aggregated, forming localized clusters without multiple patches. Samples from different domains also exhibit better agreement with each other, demonstrating better domain-invariance. Finally, the overlap between classes is also reduced, allowing for accurate classification. This demonstrates the prowess of the domain-specific batch normalization layer to aggregate different domains (sessions) together, and thereby, lead to domain (session)-invariant learning and generalization across domains (sessions).

D. Ablation Study

Table II presents the results of ablation studies with respect to different layers and kernels of the proposed model for subject 3, session 7 of NinaproDB6 dataset and subject 7

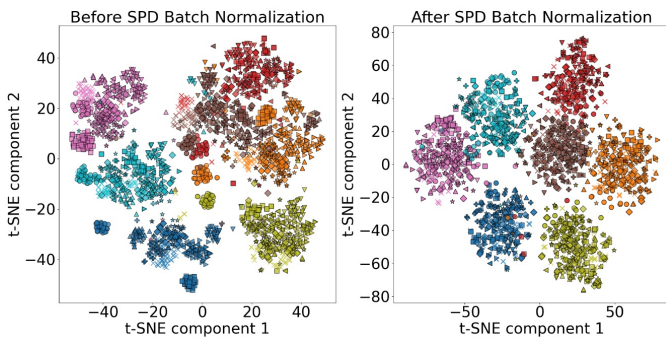


Fig. 4. t-SNE of features before and after domain-specific batch normalization for Flexwear-HD dataset. The colour of the points indicates the class, while the marker indicates the domain (\*: target domain, Others: source domain).

session 1 of Flexwear-HD dataset. The choice of the sessions (subjects) is based on the observation that their accuracies are close to the average accuracy in the respective datasets. For NinaProDB6 dataset, the overall accuracy decreases upon removal any of the layers in the Euclidean stem. This decrease in performance is highest (0.2688) when all kernels of the MSS layer are removed, followed by when all kernels of MRT are removed (0.1535). This shows the importance of MSS and MRT layers in the Euclidean stem. Further, it shows that the MSS layer designed in this article has higher contribution to the performance than the MRT layer. A kernel-wise analysis for the MSS shows that the largest performance loss is observed when either Flexor and Extensor muscle kernels or Proximal-Distal muscle kernel is removed. Thus, the muscle specific kernels, inspired from human anatomy are able to capture important discriminative information for gesture classification. A similar observation is found for F1 scores where the F1 scores are decreased by decreasing any of the Euclidean layers.

For the Flexwear-HD dataset, we observe that the removal of MRT or MSS layer reduces the performance, with higher drop for the MSS layer. Similarly, the removal of different kernels of the MSS layer reduce the performance, except for the dilated kernel. This observation points out while the proposed model produces a considerable overall performance improvement, the design of individual kernels and layers can benefit further by tuning them in a dataset-specific manner.

## VI. DISCUSSION AND CONCLUSION

*Misclassifications by TMKNet:* We investigate the types of misclassifications performed by TMKNet and show the confusion matrix for a typical case (subject 1, session 1) of NinaproDB6 dataset in Fig. 5. It can be observed that the highest number of misclassifications are made for MW (medium wrap) movement, which are mostly misclassified as AT (adducted thumb). This is followed by misclassifications for AT, most of which are predicted as MW. It is interesting to note that MW and AT have similar gesture formation patterns, i.e., thumb-vs-all-finger closing and also have nearly similar thumb adduction [26]. Thus, the mistakes made by the model are for the hand gestures that are closely related, which is a

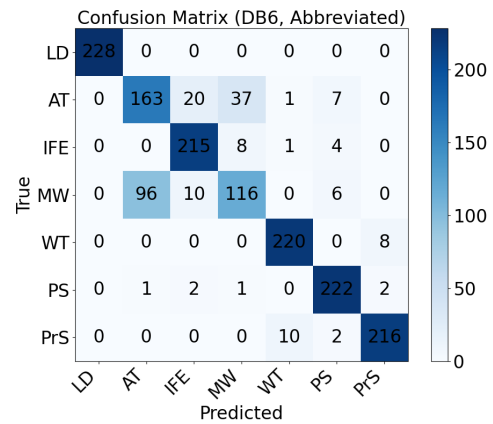


Fig. 5. Confusion matrix for NinaproDB6 (subject 1, session 1). LD: Large Diameter, AT: Adducted Thumb, IFE: Index Finger Extension, MW: Medium Wrap, WT: Writing Tripod, PS: Power Sphere, PrS: Precision Sphere.

more difficult task compared to others where the patterns are different.

*Inter-subject performance:* As discussed in Section I-B, the domain shift occurs across sessions and subjects. In this article, TSMNet was shown to provide the best performance for the inter-session scenario. We also trained TMKNet for the inter-subject scenario with both datasets, and found that the performance metrics were poorer compared to TSMNet. This can potentially be due to the choice of architecture that was optimized for inter-session performance, and further investigation is needed to correct this with a more detailed architecture search targeted at improving inter-subject performance.

*Key findings:* The proposed model with anatomy-informed multi-kernel feature extraction coupled with learning on SPD manifolds outperforms Euclidean networks and Riemannian networks for gesture classification from sEMG data for the inter-session generalizability scenario. The model is able to extract task-specific activations from different muscles that are activated differently for different tasks. The domain-specific batch normalization plays a key role in clustering features from different domains, necessary for domain generalization, while preserving separability across classes, necessary for classification. Finally, the anatomy-informed multi-kernel MSS layer proposed in the article provides the highest gain in performance.

*Outlook:* Euclidean neural networks have dominated the sEMG-based gesture decoding research. Geometric neural networks like TMKNet, operating on manifolds, can be robust for decoding hand gestures from sEMG. This work focused on inter-session generalizability with SPD layers coupled with UDA. This opens up new research avenues that can be pursued to improve the applicability in real-world settings. It was found that the same architecture does not work well for the inter-subject scenario. Further modification might be needed in this direction. The datasets used for evaluating the model contain 64 and 14 sensors for different gestures such as fine finger gestures like grip and gestures that include wrist flexion extension. Further development with more gestures is needed

TABLE II

ABLATION STUDY OF TMKNET WITH RESPECT TO DIFFERENT LAYERS AND KERNELS IN THE EUCLIDEAN STEM. THE RESULTS ARE SHOWN FOR A SAMPLE SESSION FROM A SUBJECT AND SAMPLE SESSION IN EACH DATASET. **BOLD** ENTRIES SHOW THE BEST PERFORMANCE.

Model	Accuracy		F1 score	
	NinaproDB6	Flexwear-HD	NinaproDB6	Flexwear-HD
TMKNet	<b>0.7249</b>	0.9793	<b>0.7253</b>	0.9791
w/o MRT	0.5714	0.9453	0.5687	0.9432
w/o MSS	0.4561	0.6420	0.4526	0.6388
w/o Global muscle kernel	0.7181	0.9780	0.7179	0.9777
w/o Flexor and Extensor muscle kernels	0.6955	0.9740	0.6957	0.9741
w/o Proximal-Distal muscle kernel	0.6955	0.9727	0.6957	0.9725
w/o Dilated kernel	0.7105	<b>0.9813</b>	0.7092	<b>0.9813</b>

evaluate the scalability of the model to real-life applications. While the model relies on UDA and does not need labels for the target domain, it still needs data for obtaining the batch statistics in the DSBN layer. This requirement can be further relaxed by leveraging test-time adaptation where batch statistics can be updated in real time. The model struggles to accurately classify gestures that are very similar to each other, and additional sensors such as cameras can be used to improve the performance in the multi-sensor framework.

## REFERENCES

- [1] A. Krasoulis, I. Kyranou, M. S. Erden, K. Nazarpour, and S. Vijayakumar, "Improved prosthetic hand control with concurrent use of myoelectric and inertial measurements," *Journal of neuroengineering and rehabilitation*, vol. 14, no. 1, p. 71, 2017.
- [2] S. S. Rautaray and A. Agrawal, "Interaction with virtual game through hand gesture recognition," in *2011 International Conference on Multimedia, Signal Processing and Communication Technologies*, pp. 244–247, IEEE, 2011.
- [3] G. C. S. Ruppert, L. O. Reis, P. H. J. Amorim, T. F. de Moraes, and J. V. L. da Silva, "Touchless gesture user interface for interactive image visualization in urological surgery," *World journal of urology*, vol. 30, no. 5, pp. 687–691, 2012.
- [4] K. Saurav, A. Dash, D. Solanki, and U. Lahiri, "Design of a vr-based upper limb gross motor and fine motor task platform for post-stroke survivors," in *2018 IEEE/ACIS 17th International Conference on Computer and Information Science (ICIS)*, pp. 252–257, IEEE, 2018.
- [5] H. Cao, "Unveiling the era of spatial computing," *arXiv preprint arXiv:2405.06895*, 2024.
- [6] X. Zhang, Z. Lu, C. Fan, Y. Wang, T. Zhang, H. Li, and Q. Tao, "Compound motion decoding based on semg consisting of gestures, wrist angles, and strength," *Frontiers in Neurobotics*, vol. 16, p. 979949, 2022.
- [7] J. Qi, G. Jiang, G. Li, Y. Sun, and B. Tao, "Intelligent human-computer interaction based on surface emg gesture recognition," *Ieee Access*, vol. 7, pp. 61378–61387, 2019.
- [8] A. O. Hashi, S. Z. M. Hashim, and A. B. Asamah, "A systematic review of hand gesture recognition: An update from 2018 to 2024," *IEEE Access*, vol. 12, pp. 143599–143626, 2024.
- [9] D. Korošec, "Parametric estimation of the continuous non-stationary spectrum and its dynamics in surface emg studies," *International journal of medical informatics*, vol. 58, pp. 59–69, 2000.
- [10] M. R. Al-Mulla, F. Sepulveda, and M. Colley, "A review of non-invasive techniques to detect and predict localised muscle fatigue," *Sensors*, vol. 11, no. 4, pp. 3545–3594, 2011.
- [11] K.-H. Park and S.-W. Lee, "Movement intention decoding based on deep learning for multiuser myoelectric interfaces," in *2016 4th international winter conference on brain-computer Interface (BCI)*, pp. 1–2, IEEE, 2016.
- [12] T. T. Oyemakinde, F. Kulwa, X. Peng, Y. Liu, J. Cao, X. Deng, M. Wang, G. Li, O. W. Samuel, P. Fang, *et al.*, "A novel semg-fmg combined sensor fusion approach based on an attention-driven cnn for dynamic hand gesture recognition," *IEEE Transactions on Instrumentation and Measurement*, 2025.
- [13] H. Le, G. M. Spinks, M. in het Panhuis, and G. Alici, "Cross-day myoelectric gesture recognition with hybrid multistream cnn-bidirectional lstm," in *2025 IEEE International Conference on Mechatronics (ICM)*, pp. 1–6, IEEE, 2025.
- [14] J. Shin, A. S. M. Miah, S. Konnai, S. Hoshitaka, and P. Kim, "Electromyography-based gesture recognition with explainable ai (xai): Hierarchical feature extraction for enhanced spatial-temporal dynamics," *IEEE Access*, 2025.
- [15] C. Ju and C. Guan, "Tensor-cspnet: A novel geometric deep learning framework for motor imagery classification," *IEEE Transactions on Neural Networks and Learning Systems*, vol. 34, no. 12, pp. 10955–10969, 2022.
- [16] H. T. Gowda and L. M. Miller, "Topology of surface electromyogram signals: hand gesture decoding on riemannian manifolds," *Journal of Neural Engineering*, vol. 21, no. 3, p. 036047, 2024.
- [17] S. M. Massa, D. Riboni, and K. Nazarpour, "Explainable ai-powered graph neural networks for hd emg-based gesture intention recognition," *IEEE Transactions on Consumer Electronics*, vol. 70, no. 1, pp. 4499–4506, 2023.
- [18] H. Lee, S. Lee, J. Kim, H. Jung, K. J. Yoon, S. Gandla, H. Park, and S. Kim, "Stretchable array electromyography sensor with graph neural network for static and dynamic gestures recognition system," *npj Flexible Electronics*, vol. 7, no. 1, p. 20, 2023.
- [19] D. Farina, R. Merletti, and R. M. Enoka, "The extraction of neural strategies from the surface emg," *Journal of applied physiology*, vol. 96, no. 4, pp. 1486–1495, 2004.
- [20] Y. Du, W. Jin, W. Wei, Y. Hu, and W. Geng, "Surface emg-based inter-session gesture recognition enhanced by deep domain adaptation," *Sensors*, vol. 17, no. 3, p. 458, 2017.
- [21] Y. Du, Y. Wong, W. Jin, W. Wei, Y. Hu, M. S. Kankanhalli, and W. Geng, "Semi-supervised learning for surface emg-based gesture recognition," in *IJCAI*, pp. 1624–1630, 2017.
- [22] J. Yang, M. Soh, V. Lieu, D. J. Weber, and Z. Erickson, "Emgbench: benchmarking out-of-distribution generalization and adaptation for electromyography," *Advances in Neural Information Processing Systems*, vol. 37, pp. 50313–50342, 2024.
- [23] F. Riillo, L. R. Quitadamo, F. Cavrini, E. Gruppioni, C. A. Pinto, N. C. Pastò, L. Sberini, L. Alberò, and G. Saggio, "Optimization of emg-based hand gesture recognition: Supervised vs. unsupervised data preprocessing on healthy subjects and transradial amputees," *Biomedical Signal Processing and Control*, vol. 14, pp. 117–125, 2014.
- [24] D. Brooks, O. Schwander, F. Barbaresco, J.-Y. Schneider, and M. Cord, "Riemannian batch normalization for spd neural networks," *Advances in Neural Information Processing Systems*, vol. 32, 2019.
- [25] R. Kobler, J.-i. Hirayama, Q. Zhao, and M. Kawanabe, "Spd domain-specific batch normalization to crack interpretable unsupervised domain adaptation in eeg," *Advances in Neural Information Processing Systems*, vol. 35, pp. 6219–6235, 2022.
- [26] F. Palermo, M. Cognolato, A. Gijsberts, H. Müller, B. Caputo, and M. Atzori, "Repeatability of grasp recognition for robotic hand prosthesis control based on semg data," in *2017 International Conference on Rehabilitation Robotics (ICORR)*, pp. 1154–1159, IEEE, 2017.
- [27] M. Kochurov, R. Karimov, and S. Kozlukov, "Geoopt: Riemannian optimization in pytorch," 2020.
- [28] Y. Guo, J. Liu, Y. Wu, X. Jiang, Y. Wang, L. Meng, X. Liu, F. Shu, C. Dai, and W. Chen, "semg-based inter-session hand gesture recognition via domain adaptation with locality preserving and maximum margin," *International Journal of Neural Systems*, vol. 34, no. 03, p. 2450010, 2024.

- [29] A. Dash, A. Dutta, and U. Lahiri, "Quantification of grip strength with complexity analysis of surface electromyogram for hemiplegic post-stroke patients," *NeuroRehabilitation*, vol. 45, no. 1, pp. 45–56, 2019.
- [30] L. v. d. Maaten and G. Hinton, "Visualizing data using t-sne," *Journal of machine learning research*, vol. 9, no. Nov, pp. 2579–2605, 2008.